Flutter Analysis of Anisotropic Panels with Patched Cracks

Kuo-Jiun Lin,* Pong-Jeu Lu,† and Jiann-Quo Tarn‡
National Cheng Kung University, Tainan, Taiwan, Republic of China

A finite element approach is developed to analyze the panel flutter problems of thin plate-like composite panels with patched cracks. The panel studied is a compound structure that comprises three layers including a thin cracked panel, an adhesive, and a thin patch. A 48-degree-of-freedom (DOF) triangular crack patching element is derived for numerically analyzing the compound structure. The aerodynamic pressure acting on the panel is estimated using linearized piston theory with aerodynamic damping effect neglected. By a proper tailoring of the materials, very high flutter and/or divergence boundary could usually be obtained for the composite panels. The existence of a crack usually reduces the aeroelastic stability boundary; however, some exceptions were found for the composite panel within certain range of specific filament orientation. The deterioration in flutter/divergence performance due to a crack can, in general, be cured by means of patching, and anisotropic patching is more effective as compared to the isotropic patching provided that the tailoring of the structural parameters is done correctly.

I. Introduction

A RELIABLE and accurate flutter analysis is of primary importance in the flight vehicle design. The onset of flutter would quickly develop into either catastrophic structural failure or undesirable limit cycle type oscillation. The local panel flutter of the vehicle could be essential for a global flutter to occur. For instance, the initiation of cracks in wing structure is not unusual as they may be produced by either molding, fatigue, or impact damage.[1,2] These defects could induce extremely high stresses around the cracktip regions and, thus, precipitate structural failure. When cracks are present, this local structural problem may have significant influence on the local flutter/divergence of the panel structure. The onset of the local aeroelastic instability may cause the failure of the cracked panel and cumulatively affect the global structure as well as the airload distribution and finally result in an earlier primary wing structure failure.

Recently, a work concerning the supersonic flutter behavior of isotropic thin cracked panels was conducted by Chen and Lin.[3] Their approach combines the hybrid crack/regular elements and the linearized piston theory. The fact that cracks decrease the flutter speed stimulates the present study attempting to use crack repairing to remedy the undesirable influence induced by cracks. In this regard, Mitchell et al.[4] and Jones et al.[5-8] have proposed the use of an adhesively bonded composite patch to repair flaws in metallic and/or composite structural components. Mitchell et al.[4] adopted the triangular, constant strain, plane stress finite elements for both the cracked metallic sheet and the composite overlay, together with the shear-stiffness finite element for the adhesive layer, to study the interactions between the three layers. Their computed results of strains are, for the most part, in good agreement with the experimental ones. Jones et al.[5-8] developed a crack patching finite element model to solve the stress field of a cracked composite sheet with a bonded composite patch. The model involves a triple-linear distribution of the transverse shear stresses across the thickness of the sheet-adhesive-patch compound structure. Their procedure has been successfully used in repairing static problems such as stress corrosion cracks in the wings of Hercules aircraft and fatigue cracks in the landing wheels of Macchi aircraft and in the lower wing skins of Mirage III aircraft.[9-11]

The present work attempts to develop a finite element method to study the patching repair effect on the aeroelastic characteristics of composite cracked panels. A crack patching model designed for patch-adhesive-panel compound structure is established. This model assumes a continuous triple-linear displacement field across the thickness of the compound structure, in which both patch and cracked panels are considered to be symmetrically laminated composites and modeled as thin plate-like structures. In this triple-linear displacement field, the bending and in-plane stretching displacements are uncoupled for both patch and panel components. These two different displacement fields in patch and panel are coupled through the bonding action of adhesive layer. Based on this compatible displacement field, a 48-DOF triangular crack patching finite element is constructed. This crack patching element consists of a simple 6-DOF plate stretching element (T6 element) and a high precision 18-DOF plate bending element (T18 element). The latter has been employed in conjunction with the doublet-lattice method and the linearized piston theory for the flutter analyses of composite plates in subsonic[12] and supersonic[13] flows, respectively. It has been demonstrated that the T18 element, as assisted by proper aerodynamic theory, makes a rapid convergent and accurate method in predicting the flutter boundary of thin plate-like structures.

In the present work, validity flutter and free-vibration tests are performed first for uncracked composite, cracked, and patched cracked isotropic panels. Agreement between the present computed results and those of the others[3,14-17] is obtained. The effects of composite tailoring on the flutter/divergence behavior for square cantilevered panels with or without cracks are then investigated. Finally, the patching repair of cracked panels is illustrated, and the results show substantial improvement of the flutter/divergence performance provided that aeroelastic tailoring is done correctly.

II. Analysis

The structural model considered in the present study is a compound structure shown in Fig. 1. It is made of a single patch and a through-thickness cracked panel (or sheet) bonded together by an isotropic adhesive layer. Both patch and cracked panel are assumed to be thin and symmetrically laminated composite plates. The fluid flow considered is an airstream passing over the cracked panel with an angle $\bar{\theta}$ mea-

Received Aug. 23, 1989; revision received Oct. 12, 1990; accepted for publication Nov. 15, 1990.

*Graduate Research Assistant, Institute of Aeronautics and Astronautics.

†Associate Professor, Institute of Aeronautics and Astronautics. Member AIAA.

‡Professor and Chairman, Department of Civil Engineering.

sured counterclockwise from the x axis as illustrated in Fig. 1, where θ_s and θ_p denote the composite filament angles of the sheet and the patch, respectively. The fluid entrapped on the other side under the cracked panel is assumed stationary. It is assumed that the effect of the induced acoustic phenomenon within cavity is negligible. Therefore, the linearized piston theory[18,19] is applied only on the upper side of the cracked panel when estimating the airloads acting on the compound structure.

A. Crack Patching Model

In the development of the finite element technique, the following assumptions for the crack patching model are made.

1) Both sheet and patch act as thin plates; therefore, the displacement fields of these two layers obey the classical lamination theory.

2) The transverse first derivatives of the displacement field in the adhesive layer are assumed constant.

3) The effect of crack tip singularity is not important,[3] hence, it is neglected.

4) The overlapping and contact problems on the crack faces are ignored because they can only induce local effects[20] on the global structural behavior.

Assumptions 1 and 2 simplify the displacement field that contains a continuous triple-linear distribution across the thickness of the sheet-adhesive-patch compound structural component (see Fig. 2). Therefore, the transverse shear stresses τ_{xz} and τ_{yz} exist only in the adhesive layer and are absent in the patch and sheet. This approximation may overestimate the crack tip stress intensity factors only by a few percent, as indicated by Jones and Callinan.[6] The third assumption has been shown to be acceptable by Chen and Lin[3] for panels immersed in a certain range of the flow orientation, for example, the flow orientation ranged from -30 to 30 deg with respect to the direction of fixed edge for a square isotropic cantilevered panel with edge crack.

The last assumption concerning the overlapping problem that occurred at the crack faces is actually a matter of simplifying the finite element treatment. It will be seen later that two sets of nodes should be imposed along the opposite edges of the crack interface. The displacement fields for these two sets of edge nodes are allowed to move independently to account

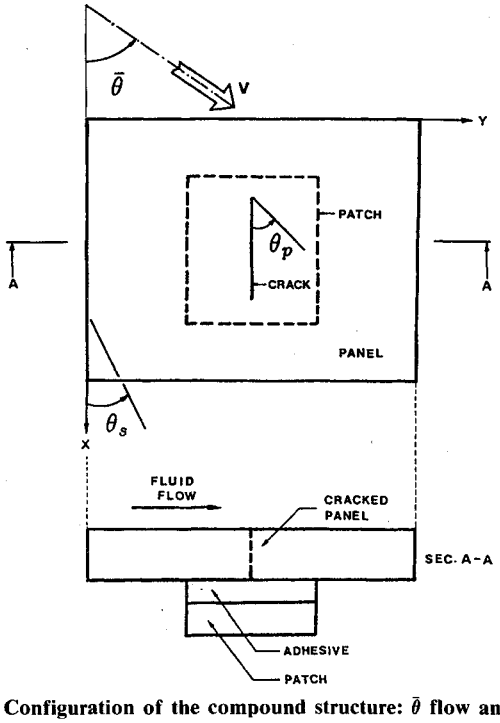

Fig. 1 Configuration of the compound structure: $\bar{\theta}$ flow angle; θ_s, θ_p composite filament angles for sheet and patch, respectively.

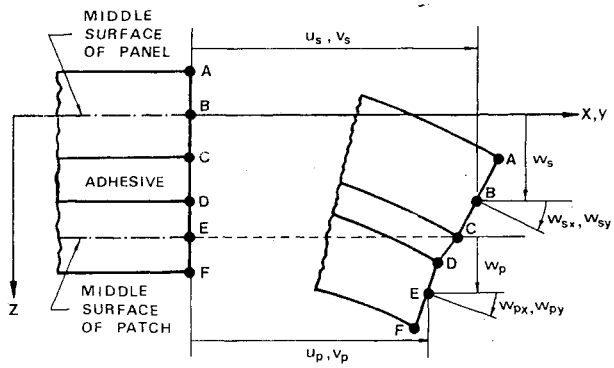

Fig. 2 Pattern of assumed deformation across the thickness of the compound structure.

for the geometric discontinuity of the crack faces. By this token, the overlapping problem may occur between these two nodes for plates undergoing bending and/or stretching motion. This, of course, is physically unrealistic. To remedy this, the contact treatment should be considered. Bowie and Freese[20] have studied these problems for both strip and infinite sheets subject to static in-plane bending. They indicate that neglecting the overlapping and contact effect may underestimate the stress intensity factor at the crack tip in the tensile field by approximately 9%. This error in local stress field is therefore realized to be of little influence when analyzing the global structural behavior such as flutter, hence, it is neglected in the present work.

Based on these assumptions, the displacement field (u,v,w) in the (x,y,z) directions within the sheet can be expressed as

$$u(x,y,z,t) = u_s(x,y,t) - z\frac{\partial w_s}{\partial x} \tag{1a}$$

$$v(x,y,z,t) = v_s(x,y,t) - z\frac{\partial w_s}{\partial y} \tag{1b}$$

$$w(x,y,z,t) = w_s(x,y,t) \tag{1c}$$

for

$$-\frac{t_s}{2} \le z \le \frac{t_s}{2}$$

where u_s, v_s, and w_s are the middle surface displacements of the sheet, t the time, and t_s the total thickness of the sheet. The middle surface of the sheet is taken to be in the plane $z=0$.

Similarly, the expressions for the displacement field within the patch can be found to be

$$u(x,y,z,t) = u_p(x,y,t) + \left(\frac{t_s}{2} + \frac{t_p}{2} + t_a - z\right)\frac{\partial w_p}{\partial x} \tag{2a}$$

$$v(x,y,z,t) = v_p(x,y,t) + \left(\frac{t_s}{2} + \frac{t_p}{2} + t_a - z\right)\frac{\partial w_p}{\partial y} \tag{2b}$$

$$w(x,y,z,t) = w_p(x,y,t) \tag{2c}$$

for

$$(t_s/2) + t_a \le z \le (t_s/2) + t_a + t_p$$

where u_p, v_p, and w_p represent the middle surface displacements of the patch and t_p and t_a denote the total thicknesses of patch and adhesive, respectively.

As for the adhesive layer, assumption 2 suggests that

$$u(x,y,z,t) = a_1(x,y,t) + b_1(x,y,t)z \tag{3a}$$

$$v(x,y,z,t) = a_2(x,y,t) + b_2(x,y,t)z \tag{3b}$$

$$w(x,y,z,t) = a_3(x,y,t) + b_3(x,y,t)z \tag{3c}$$

for

$$(t_s/2) \le z \le (t_s/2) + t_a$$

The coefficients a_i and b_i $(i=1,2,3)$ are determined from the values of the displacements u, v, and w on both interfaces of adhesive patch and adhesive sheet, which can be expressed in terms of the middle surface displacements of the patch and the sheet. The explicit form of the displacement field within the adhesive layer, hence, is found to be

$$u(x,y,z,t) = \left(1 + \frac{t_s}{2t_a} - \frac{z}{t_a}\right)u_s - \left(\frac{t_s}{2} + \frac{t_s^2}{4t_a} - \frac{t_s}{2t_a}z\right)\frac{\partial w_s}{\partial x} - \left(\frac{t_s}{2t_a} - \frac{z}{t_a}\right)u_p - \left(\frac{t_s t_p}{4t_a} - \frac{t_p}{2t_a}z\right)\frac{\partial w_p}{\partial x} \tag{4a}$$

$$v(x,y,z,t) = \left(1 + \frac{t_s}{2t_a} - \frac{z}{t_a}\right)v_s - \left(\frac{t_s}{2} + \frac{t_s^2}{4t_a} - \frac{t_s}{2t_a}z\right)\frac{\partial w_s}{\partial y} - \left(\frac{t_s}{2t_a} - \frac{z}{t_a}\right)v_p - \left(\frac{t_s t_p}{4t_a} - \frac{t_p}{2t_a}z\right)\frac{\partial w_p}{\partial y} \tag{4b}$$

$$w(x,y,z,t) = \left(1 + \frac{t_s}{2t_a} - \frac{z}{t_a}\right)w_s - \left(\frac{t_s}{2t_a} - \frac{z}{t_a}\right)w_p \tag{4c}$$

for

$$(t_s/2) \le z \le (t_s/2) + t_a$$

B. Finite Element Formulation

Once the displacement field is determined, it becomes straightforward to derive for the finite element formulation. In the present study, the high precision 18-DOF triangular plate bending element (T18 element) and the simple 6-DOF triangular plate stretching element (T6 element) are adopted respectively to simulate the bending and stretching of the compound structure.

The T18 element originally developed by Argyris et al.,[21] Bell,[22] and Cowper et al.[23] requires a large matrix inversion and integration and, hence, is time consuming in application as opposed to its advantages being conforming and accurate. Such a drawback was remedied by Stavitsky et al.[24] through the use of oblique and normal-tangential coordinate systems. Recently, Jeyachandrabose and Kirkhope[25,26] succeeded in utilizing this improved triangular T18 element to analyze the static plate bending problems. They pointed out that the convergency rate of the improved T18 element method is almost an order of magnitude faster than the ones originally presented.

The triangular T18 element assumes six deflection parameters at each vertex, namely, the lateral displacement and its first and second derivatives, resulting in a total of 18 DOF per element. The stiffness $[K_w]_e$ and mass $[M_w]_e$ matrices of the T18 element for a symmetrically laminated composite due to bending can be obtained via a standard finite element procedure (see Ref. 27 or Refs. 12 and 13 for detailed derivations). To simulate the plate stretching effect, the in-plane middle surface displacements of the composite laminate are approximated by linear functions in the construction of the T6 element. The T6 element is characterized by six in-plane middle surface displacements at the vertices, and the stiffness $[K_w]_e$ and mass $[M_w]_e$ matrices of the T6 element can be obtained readily.[27]

The derivation of the T18 and T6 elements forms a basis for developing the present finite element model of the compound structure. Since the patch layer is required to be partially adhesively bounded over the cracked region (see Fig. 1 for the schematic), there exist two types of elements in analyzing the compound structure. One is the 48-DOF triangular crack patching element (CPE element) for the patched region and the other is the 24-DOF triangular plate element (T24 element) for the unpatched region. The CPE and the T24 elements are characterized, respectively, by 48 and 24 nodal displanements at the vertices. Every vertex of a CPE element contains 16 nodal displacements, with eight displacements (six for bending and two for in-plane stretching) assigned for each patch or cracked panel component. The nodal variable vector at each vertex of a CPE element takes the following form:

$$\{q_c\} = \begin{Bmatrix} \{q_s\} \\ \{q_p\} \end{Bmatrix} \tag{5}$$

where

$$\{q_{s,p}\} = [u \quad v \quad w \quad w_x \quad w_y \quad w_{xx} \quad w_{xy} \quad w_{yy}]_{s,p}$$

The subscripts s and p represent the sheet and patch of the compound structure. Similarly, the T24 element has the same eight nodal displacements as defined for the sheet of the CPE element. By considering the displacement fields expressed in Eqs. (1), (2), and (4) together with the formulation of T18 and T6 elements, the stiffness and mass matrices of both CPE and T24 elements can be derived (see Ref. 27 for details).

CPE element:

$$[K_c]_e = \begin{bmatrix} [K_{ss}] + [K_s]_e & [K_{sp}] \\ [K_{sp}]^T & [K_{pp}] + [K_p]_e \end{bmatrix} \tag{6a}$$

$$[M_c]_e = \begin{bmatrix} [M_{ss}] + [M_s]_e & [M_{sp}] \\ [M_{sp}]^T & [M_{pp}] + [M_p]_e \end{bmatrix} \tag{6b}$$

T24 element:

$$[K_s]_e = \begin{bmatrix} [K_u]_e & [0] \\ [0] & [K_w]_e \end{bmatrix} \tag{7a}$$

$$[M_s]_e = \begin{bmatrix} [M_u]_e & [0] \\ [0] & [M_w]_e \end{bmatrix} \tag{7b}$$

in which the existence of the submatrices $[K_{ij}]$ and $[M_{ij}]$ $(i,j=s,p$; s and p denote sheet and patch, respectively) is attributed to the coupling effect of the adhesive layer (referring to Ref. 27 for their explicit expressions). Matrices $[K_p]_e$ and $[M_p]_e$ take the same form as Eqs. (7) by replacing the embedded properties of the sheet with those of the patch.

C. Aerodynamic Forces

The aerodynamic pressure acting on the compound structure is approximated using the linearized piston theory,[18,19]

$$p(x,y,t) = -\frac{2q}{\sqrt{M^2-1}}\left[\frac{\partial}{\partial \eta} + \frac{1}{V}\frac{M^2-2}{M^2-1}\frac{\partial}{\partial t}\right]w_s(x,y,t) \tag{8}$$

where p is the aerodynamic pressure, positive in the direction of the lateral deflection w_s of the panel; q the freestream dynamic pressure; V the freestream velocity defined parallel to the streamwise η axis; and M the freestream Mach number. In Eq. (8), the first term in the bracket represents the steady contribution due to local flow inclination, and the second unsteady term is associated with the effect of aerodynamic damping.

When expressed in the Cartesian coordinate system, Eq. (8) becomes

$$p(x,y,t) = -\left[\lambda\left(\frac{\partial w_s}{\partial x}\cos\bar{\theta} + \frac{\partial w_s}{\partial y}\sin\bar{\theta}\right) + \mu\frac{\partial w_s}{\partial t}\right] \tag{9}$$

where

$$\lambda = \frac{2q}{\sqrt{M^2-1}}$$

$$\mu = \lambda \frac{1}{V}\frac{M^2-2}{M^2-1}$$

The parameters λ and μ are termed the dynamic pressure parameter of the freestream and the aerodynamic damping factor, respectively.

It follows that the nonconservative aerodynamic virtual work δW^{nc} can be written in terms of the element nodal bending displacement vector associated with the panel component $\{q_{sw}\}_e$,

$$\delta W^{nc} = -\{\delta q_{sw}\}_e^T\left(\mu[C_A]_e\{\dot{q}_{sw}\}_e + \lambda[K_A]_e\{q_{sw}\}_e\right) \quad (10)$$

where $(\cdot)$ denotes a time derivative. The matrices $\mu[C_A]_e$ and $\lambda[K_A]_e$ are known as the aerodynamic damping and force matrices associated with the T18 element. The former is symmetric, whereas the latter is asymmetric; both are 18×18 matrices and can be found in Ref. 27.

D. Flutter Equations and Solution Procedure

The flutter equations that govern the dynamic stability of the aeroelastic system for the compound structure can now be obtained by employing the Hamilton's principle and the finite element assemblage process. There are two issues arising in the assemblage process that should be carefully managed. One is concerned with the crack interface (except for the crack tips) where geometric discontinuity occurs in the sheet layer. The other is concerned with the patch edge boundaries where two different structural elements (i.e., sheets with and without patch) connect. To take care of these two problems, two sets of nodes that occupy the common physical locations along the crack interface of the patch edge boundaries are imposed (see Fig. 3), respectively. In order to represent the geometric or material discontinuity appropriately, the associated nodal variables for these two sets of nodes should be kept independent from each other along the crack interface in the sheet layer. However, the nodal variables defined at the two sets of nodes lying along the patch edge boundaries or the crack location must be consistent with each other in the sheet or the patch layer. Referring to Fig. 3, the above statements are translated into the following nodal boundary requirements:

$$\{q_s\}_A = \{q_s\}_{A'} \quad (11a)$$

$$\{q_p\}_D = \{q_p\}_{D'} \quad (11b)$$

and $\{q_s\}_C$ is independent of $\{q_s\}_{C'}$.

Finishing the conduction of the assemblage process, the flutter equations for the compound structure can be obtained as[27]

$$\frac{\rho_s t_s l^4}{D_s}[M_c]\{\ddot{q}\} + \bar{\mu}[C_{cA}]\{\dot{q}\} + \left([K_c]+\bar{\lambda}[K_{cA}]\right)\{q\} = \{0\} \quad (12)$$

with

$$\bar{\lambda} = \frac{l^3}{D_s}\lambda$$

$$\bar{\mu} = \frac{l^4}{D_s}\mu$$

where $[M_c]$, $[K_c]$, $[K_{cA}]$, and $[C_{cA}]$ represent the global mass, stiffness, aerodynamic force, and aerodynamic damping matrices, respectively; l is a reference length, and D_s denotes the bending stiffness of the panel and is defined by

Isotropic panel:

$$D_s = \frac{Et_s^3}{12(1-\nu^2)} \quad (13a)$$

Anisotropic panel:

$$D_s = E_T t_s^3 \quad (13b)$$

where E, E_T, ν, and t_s are the Young's modulus, transverse Young's modulus, Poisson's ratio, and panel thickness, respectively.

The associated boundary conditions for Eq. (12) have been accounted for in the establishment of the global nodal vector $\{q\}$. For example, in Fig. 3, the boundary conditions for the nodes situated along the left fixed edge are specified by

$$u = v = w = w_x = w_y = w_{xx} = w_{xy} = 0 \quad \text{at } y = 0 \quad (14)$$

To solve the eigensystem, Eq. (12), first, the displacement vector $\{q\}$ is assumed to be

$$\{q\} = \{\bar{q}\}e^{st} \quad (15)$$

Thus, Eq. (12) becomes

$$\left(\frac{\rho_s t_s l^4}{D_s}s^2[M_c] + \bar{\mu}s[C_{cA}] + [K_c] + \bar{\lambda}[K_{cA}]\right)\{\bar{q}\} = \{0\} \quad (16)$$

Solving Eq. (16) exactly is rather time consuming. It is, therefore, advantageous to perform the modal analysis in order to reduce the large eigensystem. In doing so, Eq. (16) can then be reduced to a subsystem,

$$\left(\frac{\rho_s t_s l^4}{D_s}s^2[I] + \bar{\mu}s[C'_{cA}] + [\omega_s^2] + \bar{\lambda}[K'_{cA}]\right)\{\bar{q}\} = \{0\} \quad (17)$$

with

$$\{\bar{q}\} = [\Phi]^{-1}\{\bar{q}\}$$

$$[C'_{cA}] = [\Phi]^T[C_{cA}][\Phi]$$

$$[K'_{cA}] = [\Phi]^T[K_{cA}][\Phi]$$

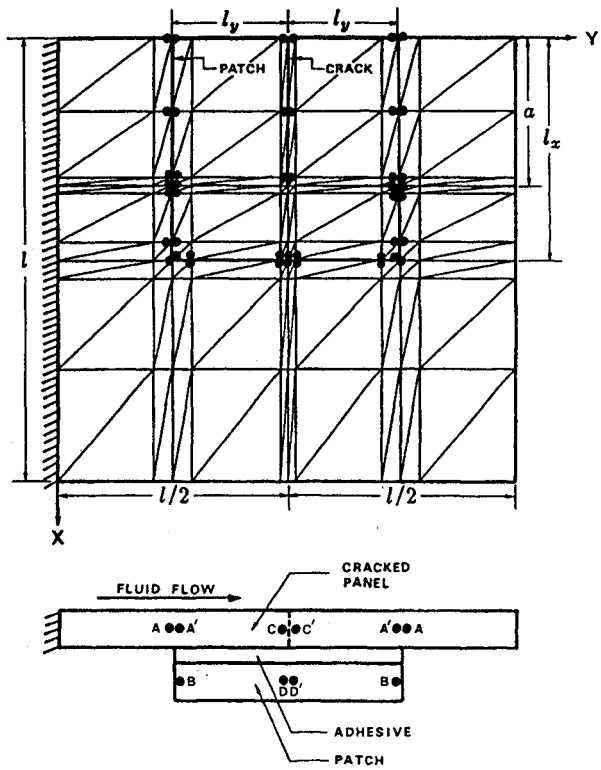

Fig. 3 Schematic of the finite element mesh for the compound structure.

where [Φ] denotes the modal matrix and the diagonal matrix $[\omega_s^2]$ contains the lower squared structural natural frequencies, typically 10, for the present finite element method.

To ease the solution procedure, Eq. (17) can be reduced to a standard form of the eigenvalue problem by introducing the transformation $\{\tilde{z}\} = s\{\tilde{q}\}$. It follows, after some manipulation, that

$$[M_E]\{X\} = s\{X\} \tag{18}$$

with

$$\{X\}^T = \lfloor \{\tilde{z}\}^T \quad \{\tilde{q}\}^T \rfloor$$

$$[M_E] = \begin{bmatrix} -\bar{\mu}[C'_{cA}] & -[\omega_s^2] - \bar{\lambda}[K'_{cA}] \\ \dfrac{\rho_s t_s l^4}{D_s}[I] & [0] \end{bmatrix}$$

Note that the dimension of the transformed system is doubled. It is noted that the eigenvalues (poles) s and the corresponding eigenvectors $\{\tilde{q}\}$ are generally complex valued due to the asymmetry of the aerodynamic force matrix.[16] The poles will start from the imaginary axis and then go into the complex plane as $\bar{\lambda}$ and $\bar{\mu}$ increase from zero. The flutter instability will be initiated when any one of the root loci crosses the imaginary axis and the corresponding value of the dynamic pressure parameter is called critical dynamic pressure and is denoted by $\bar{\lambda}_c$.

III. Numerical Investigations and Discussions

The uncracked, cracked, and patched cracked panels are examined and comparisons are made whenever required. The structures studied herein are square, and the length of the edge l is taken as the reference length scale. The parametric studies concerning the effects of filament angle and orthotropic modulus ratio of the unidirectional composites on flutter/divergence behavior are conducted. The notations used for the structural natural frequency, the critical dynamic pressure, and the corresponding frequency will be denoted by κ_s, $\bar{\lambda}_c$, and $\bar{\kappa}_c$ for isotropic panels and by κ'_s, $\bar{\lambda}'_c$, and $\bar{\kappa}'_c$ for anisotropic panels according to different expressions of D_s [see Eqs. (13a) and (13b)].

The flutter solutions presented hereafter are obtained by neglecting the aerodynamic damping effect, i.e., $\bar{\mu} = 0$. To investigate the effect of aerodynamic damping, the cases of uncracked cantilevered and fully simply supported panels have been examined in Ref. 13. For the present study of patched cracked panels, an isotropic case is tested and the result is illustrated in Fig 4. The dashed line appearing in Fig. 4 with slope $C_d = (cM/l)(M^2 - 1/M^2 - 2)$, c being the sonic speed, represents the compatibility condition between $\bar{\lambda}_c$ and $\bar{\mu}_c$. It can be seen from this figure that, for a Mach number that is sufficiently large ($M \gg 1$) or around $\sqrt{2}$, the aerodynamic damping is unimportant since the flutter dynamic pressure corresponding to the intersecting point of the dashed and solid lines departs only slightly from that of the zero damping case. Generally speaking, the damping effect is not critical for both uncracked and patched cracked panels provided that $M \gg 1$ or $M \to \sqrt{2}$. In addition, neglecting the aerodynamic damping in the calculation may frequently result in a conservative prediction of the flutter boundary. Therefore, in the subsequent parametric studies, the aerodynamic damping is set to be zero for the convenient and economical reasons, at the expense of a slight sacrifice in accuracy.

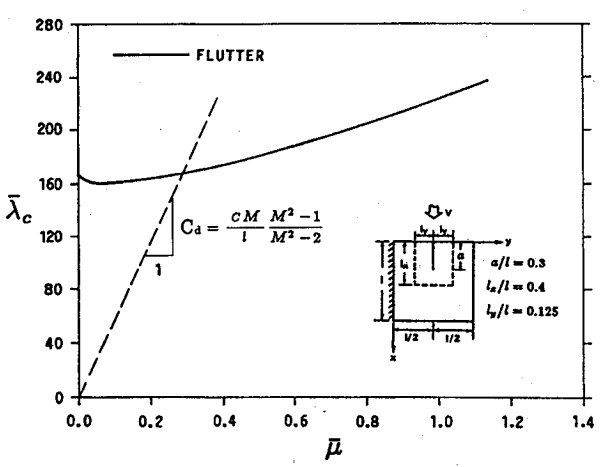

Fig. 4 Critical dynamic pressure $\bar{\lambda}_c$ vs aerodynamic damping factor $\bar{\mu}$ for a square isotropic cantilevered panel with patched edge crack in a normal flow: $t_a = 0.01t_s$; $\rho_a = 0.674\rho_s$; $E_a = 0.1E_s$; $t_p = 0.5t_s$; $\rho_p = \rho_s$; $E_p = E_s$; $\nu_s = \nu_p = \nu_a = 0.3$.

Table 1 Check of the flutter solutions for a square cantilevered panel with edge crack in a normal flow ($a/l = 0.3$)

Solutions	Number of modes	Isotropic panel, $\nu_a = 0.3$ $\bar{\lambda}_c$	Isotropic panel, $\nu_a = 0.3$ $\bar{\kappa}_c$	Anisotropic panel, $E_L/E_T = 5$, $G_{LT}/E_T = 0.4$, $\nu_{LT} = 0.25$, $\theta = 130$ deg $\bar{\lambda}'_c$	Anisotropic panel, $E_L/E_T = 5$, $G_{LT}/E_T = 0.4$, $\nu_{LT} = 0.25$, $\theta = 130$ deg $\bar{\kappa}'_c$
Present	5	43.6	25.61	3.08	5.987
T18 element	10	43.7	25.56	3.07	5.983
(32 elements)	15	43.7	25.57	3.07	5.984
Present	5	46.8	21.77	2.86	5.586
T18 element	10	46.9	21.76	2.86	5.582
(48 elements)	15	47.0	21.75	2.86	5.583
Present	5	46.4	21.42	2.80	5.491
T18 element	10	46.5	21.41	2.79	5.491
(84 elements)	15	46.5	21.43	2.79	5.492
Chen and Lin[3]	15	46.3	22.6	—	—

A. Validity Test of the Present Computer Code

1. *Uncracked Panels*

Several cases, including isotropic fully simply supported/clamped panels and anisotropic cantilevered panels in a normal oncoming supersonic flow, have been numerically investigated using the present finite element method. The results were presented elsewhere in Ref. 13. It is found that the calculated results are in good agreement with the referenced data[14-17] for both flutter and free-vibration calculations. It is worth noticing that the present T18 element method shows a monotonically convergent trend as the number of elements increases. In addition, the convergent rate of the present method is faster than the 16-DOF conforming rectangular element (CRE16 element) used by Olson,[15] the 16-DOF conforming quadrilateral element (CQ16 element) used by Sander et al.,[16] and the hybrid-stress finite element method employed by Rossettos and Tong.[17] For all of the square panels studied, a 4×4 grid mesh for a T18 element is found sufficient to yield accurate results. Therefore, at least a 4×4 grid mesh will be used in the subsequent numerical experiments.

2. *Cracked Panels*

A check on the flutter solution is made by considering a cantilevered panel with edge crack in a normal oncoming flow. The results of the critical dynamic pressure and the associated frequency parameter are listed in Table 1. For the isotropic case, the present results agree well with those obtained by the hybrid-displacement finite element method (HDFEM).[3] In addition, the use of the 48 elements together with the lowest 10 modes yields sufficient accurate solutions for both isotropic and anisotropic cases. Therefore, this scheme of finite element

arrangement and number of natural modes will be used in the following parametric studies.

3. Patched Cracked Panels

A cantilevered panel with patched edge crack (crack length $a=0.3\ell$) is illustrated in Fig. 3, where the patch to sheet area ratio is 1:10. Calculation using 10 modes is found to be sufficient to yield convergent flutter solutions for patched panels. Four different compound structures have been chosen to illustrate the effect of patch to sheet thickness ratio t_p/t_s on the flutter performance. These structures represent several combinations of the patch/sheet materials characterized by the two parameters ρ_p/ρ_s and E_p/E_s and the results are shown in Fig. 5. For instance, $\rho_p/\rho_s=1.0$ and $E_p/E_s=1.0$ indicates that the patch and the cracked panel used are of the same isotropic material. A stronger patch material and a weaker patch material are represented, typically, by $\rho_p/\rho_s=1.5$, $E_p/E_s=1.5$ and $\rho_p/\rho_s=0.5$, $E_p/E_s=0.5$. The adhesive materials used in these three structures are the same ($\rho_a=0.674\rho_s$, $E_a=0.1E_s$, $\nu_a=0.3$). In order to verify the validity of the present crack patching code, a test case of an extremely weak patch and adhesive, $\rho_p/\rho_s=10^{-2}$, $E_p/E_s=10^{-6}$ and $\rho_a=\rho_p$, $E_a=E_p$, which is expected to be very close to the unpatched case, is selected.

Curves 1, 2, and 3 in Fig. 5 approach, in the limit $t_p/t_s\to 0$, the value $\overline{\lambda_c}$, corresponding to the uncracked panel. However, for curve 4, the limiting $\overline{\lambda_c}$ value tends to match that of the unpatched cracked panel. The cause leading to these different

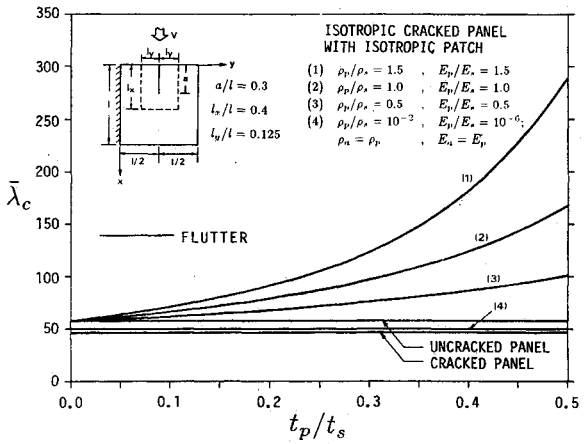

Fig. 5 Critical dynamic pressure $\overline{\lambda_c}$ vs patch to sheet thickness ratio t_p/t_s for square isotropic cantilevered panels with patched edge crack in a normal flow: $t_a=0.01t_s$; $\rho_a=0.674\rho_s$; $E_a=0.1E_s$; $\nu_s=\nu_p=\nu_a=0.3$.

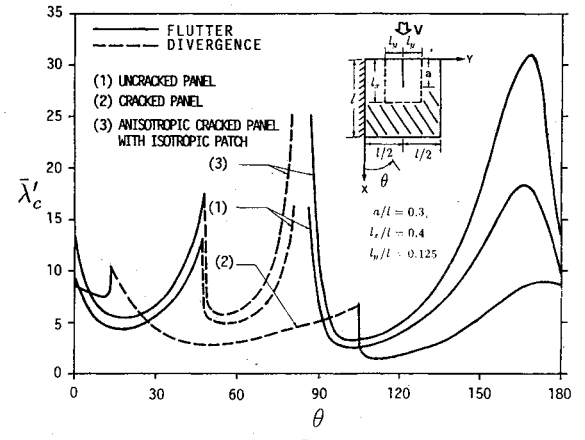

Fig. 6 Critical dynamic pressure $\overline{\lambda_c'}$ vs composite filament angle θ for square anisotropic cantilevered panels in a normal flow: $\beta=5$; $G_{LT}=0.35E_T$, $\nu_{LT}=0.3$; $t_p=0.1t_s$; $t_a=0.01t_s$; $\rho_p=1.667\rho_s$; $\rho_a=1.124\rho_s$; $E_p=3.333E_{sT}$; $E_a=0.1E_p$; $\nu_p=\nu_a=0.3$.

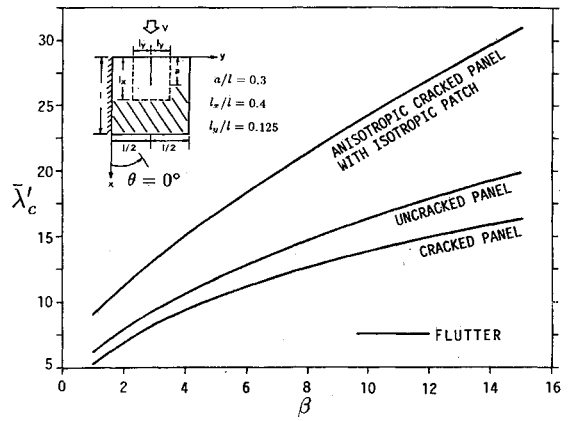

Fig. 7 Critical dynamic pressure $\overline{\lambda_c'}$ vs orthotropic modulus ratio β for square anisotropic cantilevered panels at $\theta=0$ deg in a normal flow: $G_{LT}=0.4E_T$; $\nu_{LT}=0.25$; $t_p=0.1t_s$; $t_a=0.01t_s$; $\rho_p=1.667\rho_s$; $\rho_a=1.124\rho_s$; $E_p=3.333E_{sT}$; $E_a=0.1E_p$; $\nu_p=\nu_a=0.3$.

limiting values of $\overline{\lambda_c}$, in the absence of patch, is attributed to the strengths of the adhesive layer used. Recall that the adhesive layer chosen for case 4 is extremely weak as compared to the sheet material (this implies that the adhesive is negligible), whereas in cases 1, 2, and 3, the adhesive materials used are much stronger. These results show that the adhesive layer also plays a nontrivial role in the patching of the cracked panels. For the present situation of no experimental data being available to compare with, the limiting cases of $t_p/t_s\to 0$ provide a check on the correctness of the present crack patching model and the finite element method developed.

Figure 5 also illustrates how effective crack patching is on the improvement of the flutter boundary. For the first three compound structures, the flutter performance is seen to be recovered completely when cracks are patched up. The improvement of the flutter performance by crack patching is also significant. For instance, if the patch is of the same material as the sheet with $t_p/t_s=0.5$, the weight of the structure will increase only about 5% but the critical dynamic pressure will increase to almost a triple of the original uncracked value.

B. Aeroelastic Tailoring and Crack Patching

1. Effect of Composite Filament Angle

a) *Uncracked panel.* Figure 6 shows the effect of composite filament angle on the critical dynamic pressure of a cantilevered panel in a normal oncoming airstream. Values of the orthotropic modulus ratio, in-plane shear modulus, and Poisson's ratio are chosen to be $\beta=5$ ($\beta=E_L/E_T$; E_L and E_T are the longitudinal and transverse Young's moduli, respectively), $G_{LT}=0.35E_T$, and $\nu_{LT}=0.3$. The present structural instability phenomenon (curve 1 in Fig. 6) is found to be complicated in trend. Not only flutter but also divergence type instability occurs. In the present case, divergence appears in the range around 46 deg $\le\theta\le$ 79 deg, and elsewhere the flutter takes place. Moreover, extremely high flutter and/or divergence speeds are found around $\theta=82$ deg. This phenomenon of alternating flutter and divergence instability was not reported in Rossettos and Tong's study,[17] where only the flutter-type instability is presented for a square cantilevered composite panel with filament angles running through 0–90 deg and $\beta=2$ (note that $\beta=5$ for the present case). This provides a good example for showing the complexity of the aeroelastic instability trend introduced by the directional stiffness. It is hard, and often inappropriate and dangerous, to give an overall general trend description of the aeroelastic behavior to the composite structure prior to a thorough parametric study because the parameters of composites may change the instability type and the entire structural behavior when exceeding some critical values.

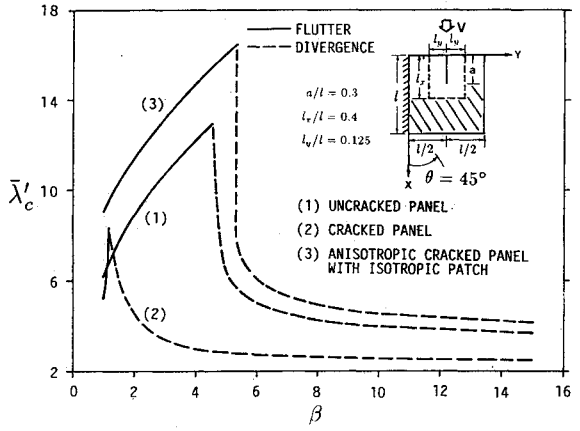

Fig. 8 Critical dynamic pressure $\bar{\lambda}'_c$ vs orthotropic modulus ratio β for square anisotropic cantilevered panels at $\theta = 45$ deg in a normal flow: $G_{LT} = 0.4E_T$; $\nu_{LT} = 0.25$; $t_p = 0.1t_s$; $t_a = 0.01t_s$; $\rho_p = 1.667\rho_s$; $\rho_a = 1.124\rho_s$; $E_p = 3.333E_{sT}$; $E_a = 0.1E_p$; $\nu_p = \nu_a = 0.3$.

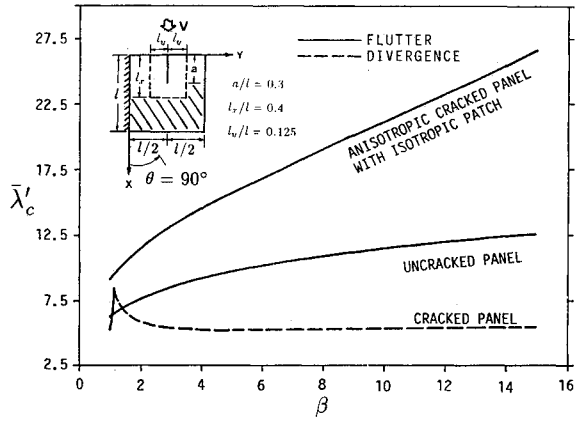

Fig. 9 Critical dynamic pressure $\bar{\lambda}'_c$ vs orthotropic modulus ratio β for square anisotropic cantilevered panels at $\theta = 90$ deg in a normal flow: $G_{LT} = 0.4E_T$; $\nu_{LT} = 0.25$; $t_p = 0.1t_s$; $t_a = 0.01t_s$; $\rho_p = 1.667\rho_s$; $\rho_a = 1.124\rho_s$; $E_p = 3.333E_{sT}$; $E_a = 0.1E_p$; $\nu_p = \nu_a = 0.3$.

b) *Cracked panel.* When an edge crack (crack length $a = 0.3\ell$) is present, it is found that the aeroelastic performance will deteriorate in general. The θ range of the divergence type instability is broadened and the extremely high flutter and/or divergence resistance for certain θ angle disappears in the case of cracked panels. It is surprising to see that for certain filament angle ranges cracked panel possesses larger critical dynamic pressure than the uncracked panel, for example, the ranges between 2 deg $\leq \theta \leq$ 27 deg and 91 deg $\leq \theta \leq$ 105 deg in Fig. 6. This indicates that the aeroelastic resistance of composite panels is not always weakened when a crack appears. This phenomenon is conjectured to be caused by the alteration of structural mode shapes induced by the crack. Usually, the directional stiffness of composites can generate mode shapes that may be favorable or detrimental to the aeroelastic performance, and when cracks are present, the situation becomes more complicated. Nevertheless, further investigation must be conducted before a precise explanation is to be made about this phenomenon.

2. Effect of Orthotropic Modulus Ratio

a) *Uncracked panel.* The effects of the orthotropic modulus ratio β on the critical dynamic pressure for three composite filament angles $\theta = 0$, 45, and 90 deg in a normal oncoming flow are depicted in Figs. 7–9, respectively, where $\beta = 1$ corresponds to the isotropic case. The results indicate that at $\theta = 0$ deg (Fig. 7) and 90 deg (Fig. 9), the critical dynamic pressures increase when β increases. However, at $\theta = 45$ deg (Fig. 8), the critical dynamic pressure first increases as β increases up to around $\beta = 4.3$, and then drops abruptly to a value lower than that of the isotropic case. Such a sudden transition is attributed to the change of the type of instability, i.e., from flutter to divergence. In this case, the use of composite materials is usually no longer beneficial.

b) *Cracked panel.* Investigation on the effect of orthotropic modulus ratio is again illustrated in Figs. 7–9 for three composite filament angles, $\theta = 0$, 45, and 90 deg. There exist some β ranges for which the critical dynamic pressure increases rather than decreases as cracks are present (see the spikes appearing in Figs. 8 and 9). These observations for composite panels are not found for the isotropic cases,[3] for which aeroelastic performance is consistently weakened when a crack exists. Generally speaking, the appearance of a crack may induce an earlier transition of instability from flutter to divergence or change the type of instability as shown in Figs. 8 and 9, which will result in a substantial decrease in the critical dynamic pressure as β increases further.

3. Effect of Crack Patching

a) *Anisotropic cracked panel with isotropic patch.* In Figs. 6–9, the effects of the use of isotropic patch are illustrated, where the critical dynamic pressures are plotted against either the composite filament angle or the orthotropic modulus ratio of the anisotropic cracked panel. All of the results show that the curves of critical dynamic pressure for the patched panels generally follow the same trend as those for the uncracked panels. Moreover, the magnitudes of the critical dynamic pressure usually are enlarged after patching when compared to the uncracked and cracked panels. These indicate that the use of isotropic patch may enhance the aeroelastic performance of the anisotropic cracked panel.

b) *Isotropic cracked panel with anisotropic patch.* The effect of composite filament angle θ_p of the patch on the critical dynamic pressure of an isotropic cracked panel is illustrated in Fig. 10. It is observed that the improvement provided by the composite patch fluctuates as the composite filament angle varies. Except for a small filament angle range between 107 deg $\leq \theta_p \leq$ 122 deg, using the composite patch is found superior once tailoring is done correctly. For the present case, the optimal tailoring of the composite patch occurs as the filaments are oriented around $\theta_p = 64$ and 159 deg.

c) *Anisotropic cracked panel with anisotropic patch.* The case considered herein is a cracked panel and a patch made of the same composite material. The free parameter, therefore, is

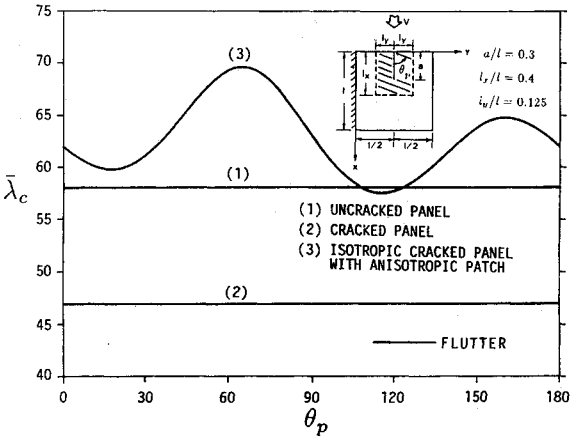

Fig. 10 Critical dynamic pressure $\bar{\lambda}_c$ vs composite filament angle of patch θ_p for a square isotropic cantilevered edge cracked panel with anisotropic patch in a normal flow: $t_p = 0.1t_s$; $t_a = 0.01t_s$; $\rho_p = 0.6\rho_s$; $\rho_a = 0.674\rho_s$; $E_a = 0.1E_s$; $E_{pT} = 0.3E_s$; $\beta_p = 5$; $G_{pLT} = 0.35E_{pT}$; $\nu_s = \nu_{pLT} = \nu_a = 0.3$.

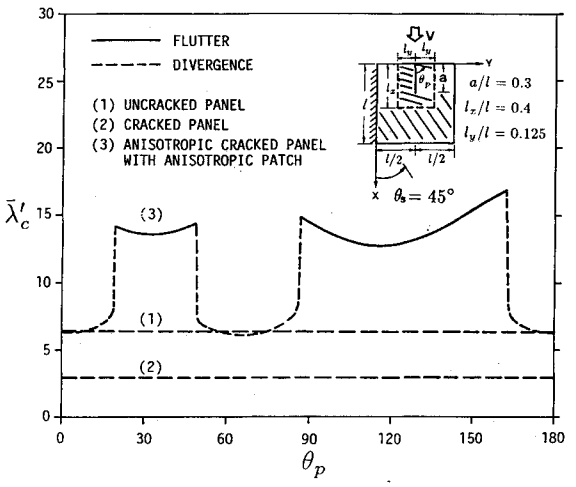

Fig. 11 Critical dynamic pressure $\bar{\lambda}'_c$ vs composite filament angle of patch θ_p for a square anisotropic cantilevered edge cracked panel with anisotropic patch in a normal flow: $t_p = 0.1t_s$; $t_a = 0.01t_s$; $\rho_p = \rho_s$; $\rho_a = 1.124\rho_s$; $\beta_s = 5$; $G_{sLT} = 0.4E_{sT}$; $E_a = 0.333E_{sT}$; $E_{pT} = E_{sT}$; $\beta_p = 5$; $G_{pLT} = 0.4E_{pT}$; $\nu_{sLT} = \nu_{pLT} = 0.25$; $\nu_a = 0.3$.

the relative composite filament angle between the panel and patch. Figure 11 illustrates this effect by rotating the patch while holding the panel filament orientation fixed. Generally speaking, employing patch over cracked panel can almost always improve the stability bound. It is also found that the instability type for the patched cracked panel alternates when the filament angle of patch moves across the four transition points, i.e., $\theta_p = 19$, 48, 87, and 163 deg. Jumps of the critical dynamic pressure take place at these transition points. An originally divergence bounded panel can become flutter bounded, and this introduction of instability type change provided by composite patching may remarkably improve the aeroelastic performance.

IV. Conclusions

A finite element discretization of the sheet-adhesive-patch compound structure, together with the aerodynamic piston theory, is established to examine the effect of patching on the panel flutter characteristics. Sufficient validity tests have been performed and checked with the available computational data. Excellent agreements in both free-vibration and flutter examinations are obtained. A series of numerical studies have been conducted for square cantilevered unidirectional composite panels. The effects of composite filament angle and orthotropic modulus ratio on the flutter/divergence characteristics of panels with/without cracks were examined first. The repairing effect of patching on the flutter/divergence characteristics of the cracked panel was then studied. As a whole, patching can make the panel structure even more aeroelastically resistant than before, but the optimal results can only be achieved by a careful structural tailoring. Based on the parametric investigation performed, the following concluding remarks are made.

1) Effect of composite filament angle: For a cantilevered panel, a particular alternating flutter-divergence-flutter type instability, which is not observed in the isotropic materials, shows up as the filament orientation varies.

2) Effect of orthotropic modulus ratio: In general, a higher flutter boundary can be achieved by increasing the orthotropic modulus ratio. However, reverse trend in critical speed may occur if the instability type is abruptly changed.

3) Effect of crack: The flutter performance will deteriorate once a crack appears in the isotropic panel. From the cases studied in the present work, it was discovered, unlike the isotropic panel, that the existence of a crack may sometimes result in the increase of flutter or divergence boundary for composite panels.

4) Effect of patching repair: The deterioration of the aeroelastic performance due to a crack can be effectively cured by means of isotropic or anisotropic patching with slight penalty on the structural weight. The patching repaired panel can at least retrieve the original aeroelastic characteristics, or achieve a better performance if tailoring is done correctly.

Acknowledgments

This work was supported by the National Science Council under Contract CS 77-0210-D006-14. The authors would like to thank Yuan-Bin Chang of the Aeronautical Research Laboratory for many valuable discussions.

References

[1]Verette, R. M., and Demuts, E., "Effects of Manufacturing and In-Service Defects on Composite Materials," Army Material and Mechanics Research Center, MS 76-Z, 1976, pp. 123–136.

[2]Hoffman, G. A., and Konishi, D. Y., "Characterization of Manufacturing Flaws in Graphite-Epoxy," Army Material and Mechanics Research Center, MS 77-5, pp. 5.1.1–5.1.1.3, 1977.

[3]Chen, W. H., and Lin, H. C., "Flutter Analysis of Thin Cracked Panels Using the Finite Element Method," *AIAA Journal,* Vol. 23, No. 5, 1985, pp. 795–801.

[4]Mitchell, R. A., Woolley, R. M., and Chwirut, D. J., "Analysis of Composite-Reinforced Cutouts and Cracks," *AIAA Journal,* Vol. 13, No. 6, 1975, pp. 744–749.

[5]Jones, R., and Callinan, R. J., "On the Use of Special Crack Tip Elements in Cracked Elastic Sheets," *International Journal of Fracture,* Vol. 13, 1977, pp. 51–64.

[6]Jones, R., and Callinan, R. J., "Finite Element Analysis of Patched Cracks," *Journal of Structural Mechanics,* Vol. 7, No. 2, 1979, pp. 107–130.

[7]Jones, R., and Aggarwal, K. C., "Analysis of Bonded Repairs to Damaged Fibre Composite Structures," *Engineering Fracture Mechanics,* Vol. 17, No. 1, 1983, pp. 37–46.

[8]Jones, R., Bailey, R., and Roberts, J. D., "Computational Methods in Modern Repair Technology," *Computational Mechanics,* Vol. 2, 1987, pp. 247–252.

[9]Baker, A. A., "A Summary of Work on Applications of Advanced Fibre Composites at the Aeronautical Research Laboratories," Composites 9, Australia, 1978, pp. 11–16.

[10]Baker, A. A., Callinan, R. J., Davis, M. J., Jones, R., and Williams, J. G., "Application of BFRP Crack Patching to Mirage III Aircraft," *Proceedings of the 3rd International Conference on Composite Materials,* Paris, France, 1980, pp. 1424–1438.

[11]Jones, R., and Callinan, R. J., "Analysis and Repair of Flaws in Thick Structures," *Proceedings of the 5th International Conference on Fracture,* Cannes, France, April 1981, Advances in Fracture Research 1, 1981, pp. 23–33.

[12]Lin, K. J., Lu, P. J., and Tarn, J. Q., "Flutter Analysis of Cantilever Composite Plates in Subsonic Flow," *AIAA Journal,* Vol. 27, No. 8, 1989, pp. 1102–1109.

[13]Lin, K. J., Lu, P. J., and Tarn, J. Q., "Flutter Analysis of Composite Panels Using High-Precision Finite Elements," *Computers & Structures,* Vol. 33, No. 2, 1989, pp. 561–574.

[14]Houbolt, J. C., "A Study of Several Aerothermoelastic Problems of Aircraft Structures in High Speed Flight," Ph.D. Dissertation, Swiss Federal Inst. of Technology, Zurich, Switzerland, 1958.

[15]Olson, M. D., "Some Flutter Solutions Using Finite Elements," *AIAA Journal,* Vol. 8, No. 4, 1970, pp. 747–752.

[16]Sander, G., Bon, C., and Geradin, M., "Finite Element Analysis of Supersonic Panel Flutter," *International Journal for Numerical Methods in Engineering,* Vol. 7, 1973, pp. 379–394.

[17]Rossettos, J. N., and Tong, P., "Finite-Element Analysis of Vibration and Flutter of Cantilever Anisotropic Plates," *Journal of Applied Mechanics,* Vol. 41, Dec. 1974, pp. 1075–1080.

[18]Ashley, H., and Zartarian, G., "Piston Theory—A New Aerodynamic Tool for the Aeroelastician," *Journal of the Aeronautical Sciences,* Vol. 23, No. 12, 1956, pp. 1109–1118.

[19]Dugundji, J., "Theoretical Considerations of Panel Flutter at High Supersonic Mach Numbers," *AIAA Journal,* Vol. 4, No. 7, 1966, pp. 1257–1266.

[20]Bowie, O. L., and Freese, C. E., "On the 'Overlapping' Problem in Crack Analysis," *Engineering Fracture Mechanics,* Vol. 8, 1976, pp. 373–379.

[21]Argyris, J. H., Fried, I., and Scharpf, D. W., "The TUBA Family of Plate Elements for the Matrix Displacement Method," *The Aero-*

nautical Journal of the Royal Aeronautical Society, Vol. 72, 1968, pp. 701–709.

[22]Bell, K., "A Refined Triangular Plate Bending Finite Element," *International Journal for Numerical Methods in Engineering,* Vol. 1, 1969, pp. 101–122.

[23]Cowper, G. R., Kosko, E., Lindberg, G. M., and Olson, M. D., "Static and Dynamic Applications of a High-Precision Triangular Plate Bending Element," *AIAA Journal,* Vol. 7, No. 10, 1969, pp. 1957–1965.

[24]Stavitsky, D., Macagno, E., and Christensen, J., "On the Eighteen Degrees of Freedom Triangular Element," *Computer Methods in Applied Mechanics and Engineering,* Vol. 26, 1981, pp. 265–283.

[25]Jeyachandrabose, C., and Kirkhope, J., "Explicit Formulation for the High Precision Triangular Plate-Bending Element," *Computers & Structures,* Vol. 19, No. 4, 1984, pp. 511–519.

[26]Jeyachandrabose, C., and Kirkhope, J., "Explicit Formulation for a High Precision Triangular Laminated Anisotropic Thin Plate Finite Element," *Computers & Structures,* Vol. 20, No. 6, 1985, pp. 991–1007.

[27]Lin, K. J., "Flutter Analysis of Composite Plates with Patched Cracks," Ph.D. Dissertation, Inst. of Aeronautics and Astronautics, National Cheng Kung Univ., Taiwan, ROC, July 1988.